

pubs.acs.org/est Article

Direct Measurements of the Forces between Silver and Mica in Humic Substance-Rich Solutions

Janis E. Patiño, Tonya L. Kuhl, and Verónica L. Morales*



Cite This: Environ. Sci. Technol. 2020, 54, 15076-15085



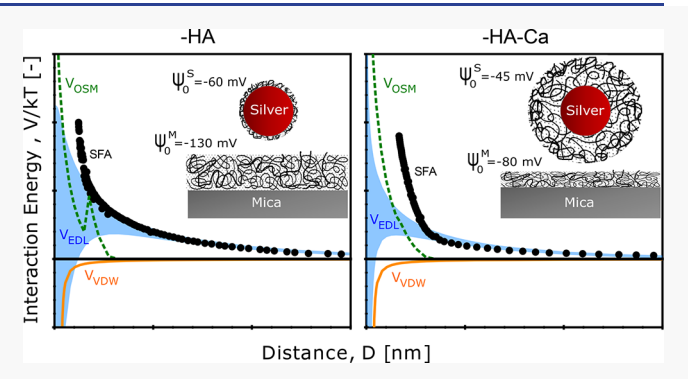
ACCESS

Metrics & More

Article Recommendations

3 Supporting Information

ABSTRACT: Deposition of engineered nanoparticles onto porous media from flowing suspensions is important for soil and groundwater quality. The deposition mechanism is controlled by interaction forces between particles and collectors. We investigated the origin and magnitude of opposing forces between silver and mica surfaces (representing nanosilver and sand grains) in solutions relevant to agricultural soils with direct measurements using a surface force apparatus. Solutions of variable NaNO₃, Ca(NO₃)₂, and humic acid (HA) concentrations were used to differentiate individual contributing forces and quantify surface properties. The measured Hamaker constant for silver—water—mica was consistent with Lifshitz theory. Our results indicate that HA forms an adsorbed surface layer, but its charge, thicknesses,



compressibility, and mass are significantly larger on mica than silver. Ca²⁺ primarily reduced the differences between the initially adsorbed HA layer properties on each surface, making them more similar. Force—distance profiles indicate that, when silver—mica systems were exposed to HA, osmotic—steric, electrostatic, and van der Waals forces dominate. Soft particle theory was deemed inappropriate for this system. Derjaguin's approximation was utilized to translate force measurements into interaction energy between nanosilver particles and mica collectors. We propose attachment efficiency estimates from measured surface properties, which suggest high particle mobility when nanosilver is applied to HA-rich agricultural soils with modest ionic strength.

■ INTRODUCTION

The expanding application of engineered nanoparticles (ENPs) in medical products, textiles, paints, cleaning agents, electric appliances, and cosmetics is increasing their presence in the natural environment. 1-5 Nanosilver (n-Ag) in particular is broadly used because of its biocidal properties.⁶⁻⁸ Several studies have found that n-Ag erodes from consumer products and is released into wastewater treatment plants, where it is removed from the wastewater and accumulated in the sludge. 1,3,9,10 In the United States, sludge is commonly applied to agricultural soils to recycle nutrients, which serves as a major entry route for ENPs into soil and water environments. 11,12 Excessive n-Ag release into the subsurface raises concerns regarding the impact it could have on the quality of groundwater used for potable water production and the potential toxic or detrimental effects on beneficial soil microorganisms. 13-16 Toxicity mitigation of n-Ag toward soil bacteria has been observed when ENPs are coated with humic acid and other organic materials in soil pore water. 17 Understanding the transport and fate processes of ENPs in natural matrices like agricultural soils is therefore essential to the protection and future use of soil and groundwater resources.

Transport and deposition of suspended particles onto the surface of porous media is commonly modeled with colloid

filtration theory (CFT). In CFT, deposition is described as a first-order kinetic process that depends on two sequential steps. First, the single-collector contact efficiency, η_0 , captures the mass transfer rate from the bulk fluid to the solid surface controlled by diffusion, interception, and sedimentation. Second, the attachment efficiency, α , captures the energy of interaction between the particle and the solid. Classic Derjaguin–Landau–Verwey–Overbeek (DLVO) theory, and extensions to it (e.g., Ohshima, Grasso et al., Dwivedi et al., 22–24 and references therein), are the gold standard for describing the additive attractive and repulsive interactions as a function of separation distance. The one-dimensional form of CFT describes colloid concentration, C, in time and space as

$$\frac{\partial C}{\partial t} = D \frac{\partial^2 C}{\partial x^2} - \nu \frac{\partial C}{\partial x} - k_{\rm d} C \tag{1}$$

Received: August 8, 2020 Revised: September 26, 2020 Accepted: October 27, 2020 Published: November 10, 2020





where D and v are the dispersive and advective terms, respectively. k_d is the irreversible deposition rate coefficient, which is related to contact and attachment efficiency terms via 25,26

$$k_{\rm d} = \frac{3}{4} \frac{(1-\theta)}{R_{\rm M}} v \alpha \eta_0 \tag{2}$$

Here, θ is the porosity of the medium, and $R_{\rm M}$ is the mean radius of the soil grains (collectors). While η_0 can be evaluated from well-accepted correlations, ^{18,27} there is not yet a similarly accepted and general correlation to determine α from suspension properties or DLVO profiles, although several different approaches have been proposed. ^{28–32} Specifically, a general validated model for α that describes both bare and polymer-coated particles is still lacking.

Deposition of ENPs within the soil environment by either individual particles or homoaggregates/heteroaggregates is greatly influenced by the combined effects of solution ionic strength (IS), ionic composition, pH, stabilizing agent, and organic matter.4 Macromolecular interactions with dissolved organic matter (DOM), such as humic and fulvic acids in soil pore water, have been found to have a profound impact on ENP stability in terrestrial and aquatic environments. 33-37 On one hand, humic substances readily adsorb to surfaces and act as stabilizing agents for colloids and ENPs in DOM-rich solutions, 38-40 thereby potentially altering their transport in granular media. 41,42 On the other hand, the presence of Ca2+ modifies ENP-DOM complexes through cation bridging, which can cause charge neutralization or reversal and enhance retention with delayed breakthrough. 43,44 Despite numerous studies of aggregation, adsorption, and deposition of ENPs with DOM, 42,45-49 direct quantification of the relative contribution from specific interactions between the surfaces of ENPs and soil grain forces at work in ENP-DOM complexes (van der Waals, electrostatic, osmotic-steric, elastic-steric, etc.) to the resulting total force and, thus, to particle deposition, is lacking. This is due in part to the limited experimental methods available to directly evaluate colloidal forces (e.g., by atomic force microscopy 50 or surface force apparatus⁵¹), substantial guess-work involved in modeling the theoretical energy of interaction, and difficulty in properly characterizing adsorbed layer properties needed to parametrize existing models. Such information is highly dependent on the characteristics of the bare substrates and is required to parametrize transport models to improve particle migration predictions. These knowledge gaps are addressed in this study.

The objective of this work was to directly measure the interaction force profile between silver and mica surfaces in solutions representative of agricultural soils. The actual surface potentials, DOM adsorbed layer thickness, and compressibility, as well as total colloid forces were determined experimentally. Separation of the force profiles into their individual contributions allowed us to establish their origin. The measured force profiles for different solution conditions were translated into energy of interaction profiles for cases of n-Ag particles interacting with sandlike collectors. Each suspension's expected attachment efficiency was parametrized by precise measurements of surface and adsorbed layer properties and modeled with CFT.

MATERIALS AND METHODS

Materials. Measurements were made under three different solution conditions. The first (termed "control") was composed of an electrolyte solution of 0.5 mM NaNO3 (99.995%, Sigma, St. Louis, MO) to define the physical contact between the surfaces and their surface charge properties. The second (termed "-HA") was composed of 0.5 mM NaNO₃ with 20 mg/L Eliott Soil humic acid (HA) (International Humic Substances Society, St. Paul, MN). The concentration of 20 mg/L was selected to mimic DOM-rich groundwater conditions (18-20 mg C/L).⁵² The third (termed "-HA-Ca") was composed of 0.5 mM NaNO₃, 0.25 mM Ca(NO₃)₂ (99.995%, Sigma, St. Louis, MO), and 20 mg/ L HA. Milli-Q gradient water (resistivity of 18 M Ω ·cm) was used to prepare the solutions, and the pH was adjusted to 7 by addition of NaOH. The surfaces studied were silver and ruby muscovite mica (S&J Trading, New York), which are described in detail in the next section. Silver particles of 100 nm diameter stabilized with sodium citrate (Sigma-Aldrich) were used in ζ potential measurements.

Surface Force Measurements. A custom-automated surface force apparatus (SFA) was used to measure interaction forces between silver and mica surfaces. This methodology was chosen, because it allows for direct and precise measurements at separation distances down to 0.1 nm, thus providing a "ground truth force profile" of the system. 53 Additionally, the use of SFA facilitated the definition of an absolute reference for contact between the surfaces, which is a limitation of alternative methodologies. SFA uses multiple-beam interferometry to directly measure surface separation and contact geometry. 54 The technique is described in detail elsewhere. 51,53,55 Briefly, one surface (mica) was mounted on a fixed stage, while the second (mica/silver) was mounted on a double-cantilever spring of known stiffness ($\sim 2.4 \times 10^{-5}$ mN/ m), which can be displaced vertically. Mica was chosen as the model for collector in porous media, because it is a layered alumina-silicate mineral that can be cleaved along the basal plane <001> to yield a molecularly smooth surface of uniform thickness (here 2-3 μ m) over large areas. Due to its atomic smoothness, mica is an ideal substrate for high-resolution force profile measurements of adsorption layers. It is noted that nanoscale roughness is prevalent in the subsurface and has been shown to affect ENP transport. 56 Nevertheless, the aim of our work is on better characterizing the force responsible for attachment for HA-coated surfaces. Importantly, for studies of HA adsorption, the basal plane of mica has negatively charged lattice sites, similar in density to those of highly negatively charged silica or sand.⁵⁷ Mica surfaces were coated on one side with a 55 nm thick silver layer deposited by evaporation (Alfa Asear 99.99%). This layer permits the partial transmission of light normally directed through the surfaces, which constructively interferes and produces fringes of equal chromatic order (FECO) for surface separation determination.

Within 2 days of depositing the silver coating, the surfaces were glued onto a cylindrical lens and mounted into the SFA. Contact in air was measured. Afterward, the SFA was filled with one of the three aqueous solutions and allowed to equilibrate for at least 2 h for measurements in control solution and at least 24 h for measurements in the -HA and -HA-Ca solutions in a temperature-controlled room at 25 °C. Minimal hysteresis was observed between subsequent force profile measurements (compare approach and separation in Figure 1)

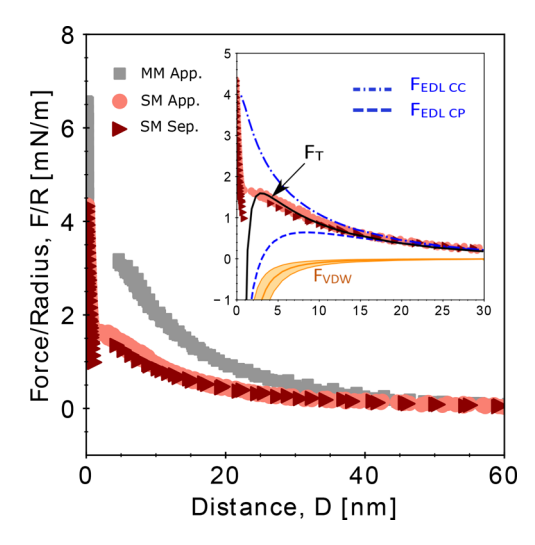


Figure 1. Force—distance profiles between opposing mica—mica (gray markers) and silver—mica (red markers) surfaces in the control solution. D=0 nm is defined as the contact between the surface pairs. Inset shows the predicted electric double layer at constant charge $(F_{\rm EDLCC})$ and constant potential $(F_{\rm EDLCP})$ boundary conditions, as well as van der Waals $(F_{\rm VDW})$ contributions to the total force for the silver—mica experiments.

indicating that the force measurements were carried out at essentially equilibrium conditions. Two configurations of silver-coated mica surfaces were used. In the symmetric configuration, the silver coating faced the back of both surfaces to measure mica-mica forces. In the asymmetric configuration, the silver coating faced the front of one surface and the back of the other surface to measure silver-mica forces. Determination of forces between the surfaces in a cross cylinder configuration was obtained from the deflection of the cantilever spring supporting the lower surface.⁵³ The distance between the surfaces (D) was measured by the position of FECO peak wavelengths within a spectrometer using a computerautomated acquisition system. Final data obtained from the SFA consisted of force profiles as a function of separation distance between the two surfaces. The measured force between crossed cylinders was normalized by the geometric mean radius of curvature, R. At least two independent SFA experiments were carried out for each configuration and solution combination tested. The results below show one representative data set, but replicates were consistent.

Interpretation of SFA Data. The following describes the approach followed to separate the individual force contributions to the net force measured by SFA. Repulsive electrostatic double layer force, $F_{\rm EDL}/R$, contributions were determined for each experiment by numerically fitting the nonlinear Poisson—Boltzmann (NLPB) model to SFA data for D>10 nm, where the interacting forces were purely electrostatic. The effective Debye length, κ^{-1} , was determined from the exponentially decaying force and compared to the expected κ^{-1} based on solution properties. Deviations enabled an estimate of HA's contribution to the system's overall electrostatics. Attractive van der Waals force, $F_{\rm VDW}/R$, contributions were obtained from the control solution data, after subtracting the electrostatic force. The van der Waals attractive force is the same across all experiments of equivalent surface configuration. The Hamaker constant, A, for the silver—water—mica system was determined as 53

$$\frac{F_{\text{VDW}}}{R} = -\frac{A}{6D^2} \tag{3}$$

Additional repulsive force contributions from adsorption of HA were estimated as the residual after subtraction of both the fitted electrostatic and van der Waals forces (classic DLVO) from SFA measurements of the total interaction force profile.

Electrophoretic mobility values were collected on nanosilver suspensions matching the solutions described above using the ZetaPlus analyzer (Brookhaven Instruments Corp., Holtsville, NY). Ten measurements were collected for each sample, with replicate samples for each solution. ζ -potentials (ζ) were determined from average electrophoretic mobilities using the Smoluchowski equation. These values were compared to the surface potential data obtained from the SFA measurements.

■ RESULTS AND DISCUSSION

Interaction Forces. Control Solution. Measured force profiles in the control solution (no HA) between opposing silver—mica (red markers) and mica—mica surfaces (gray markers) are shown in Figure 1. Classic DLVO surface forces are observed with long-range electrostatic repulsion and short-range van der Waals attraction. The adhesive contact of the surfaces in air was defined as D=0 nm. We note that the mica—mica contact is well-defined for molecularly smooth surfaces. The mica—silver contact, however, was slightly compressible (i.e., the surfaces were elastically flattened upon compression), consistent with a surface roughness of ~5 Å on the silver surface from evaporation deposition.

Electrostatic repulsion is captured by the NLPB model, whereby the boundary conditions of constant charge or constant potential describe the two extremes. Real systems lie somewhere in between due to charge regulation, ⁵⁹ as is shown in the inset of Figure 1. The control data more closely resemble a constant charge behavior (as described in the next section). The empirically determined effective κ^{-1} in the control solution was 14 ± 0.3 nm, consistent with the expected value from solution properties (see Table 1). Semilog plots showing κ^{-1} for each solution are shown in Figure S1.

The van der Waals attraction is obtained from data with the control solution and is assumed to be the same across all experiments of equivalent surface configuration. The Hamaker constant for silver—mica interacting through water has a range of $A = [2.2, 6.4] \times 10^{-20}$ J, consistent with Lifshitz theory estimations of $A = 4.2 \times 10^{-20}$ J. Consistent with Lifshitz theory estimations of $A = 4.2 \times 10^{-20}$ J. Uncertainty in A is reflected in the orange shaded region of van der Waals attractive forces shown in the inset of Figure 1. Both constant charge and constant potential fits to the data are shown. The best fit to the total profile is obtained with constant charge and $A = 4.3 \times 10^{-20}$ J (middle line in shaded region) as demonstrated by the solid line, $F_{\rm T}$. The value of A was assumed constant across experiments based on refractive index measurements (data not shown), whose results were equivalent in the control and HArich solutions.

-HA and -HA-Ca Solutions. Measured force profiles in the -HA (green circles) and -HA-Ca (blue squares) solutions between opposing mica—mica and silver—mica surfaces are shown in Figure 2, in parts a and b, respectively. Generally, the force maximum is higher for the symmetric compared to the asymmetric system, signaling that HA adsorption on mica is greater than on silver and that the solution composition impacts the adsorption behavior. Long-range electrostatic repulsion was well-described by the NLPB model at constant

Table 1. Summary of Charge and Adsorbed Layer Properties for Silver and Mica Surfaces at Each Tested Solution Composition^a

		solution composition		
parameter		control	-HA	-HA-Ca
κ^{-1} expected	[nm]	13.5	13.5	11.1
κ^{-1} effective	[nm]	14 ± 0.3	12 ± 0.2	10 ± 0.8
IS expected	[mM]	0.5	0.5	0.75
IS effective	[mM]	0.47	0.64	0.92
$\psi_0^{ m M}$	[mV]	-110 ± 10	-130 ± 20	-80 ± 10
ψ_0^{S}	[mV]	-50 ± 5	-60 ± 5	-45 ± 5
ζ_s^b	[mV]	-52 ± 4	-61 ± 3	-44 ± 3
L_{M}	[nm]	0	5.5	2.4
L_S	[nm]	0	0.5	4.4
$\lambda_{ ext{M}}$	[%]	0	48.8	14.5
$\lambda_{ m S}$	[%]	0	53.8	66.0
Γ_{M}	$[mg/m^2]$	0	2.24	2.24
$\Gamma_{\rm S}$	$[mg/m^2]$	0	0.18	1.19

 $^{\alpha}\kappa^{-1}$ is the Debye length, ψ_0 is the surface potential, ζ is the ζ -potential, L is the uncompressed adsorbed HA layer thickness, λ is the layer's compressibility, and Γ is the estimated mass of adsorbed HA. The subscripts and superscripts indicate the surface type as mica (M) or silver (S). b Values measured for 100 nm silver nanoparticles.

charge boundary conditions (shown by the solid, dotted, and dashed lines for the control, -HA, and -HA-Ca solutions, respectively). Distances where the force measurements deviated from a purely electrostatic interaction (arrows) denote the onset of repulsion due to adsorbed HA. We note that it was impossible to bring the surfaces into contact (D = 0)nm) due to the HA adsorption layers and hydrating water. Importantly, for both solutions, short-range van der Waals attraction is masked by the overwhelming net repulsive forces imparted by electrostatics and adsorbed HA. This is discussed in greater detail below. The effective κ^{-1} (see Table 1) for -HA was 2 nm lower than for the control solution and its expected value, signifying an increase in IS due to a release of ions from charged HA functional groups. Similarly, for -HA-Ca, the effective κ^{-1} was lower than its expected value. The effective IS in solutions containing HA was ~0.16 mM higher than was expected (from only added salt), accounting for the ions released from HA. It should be noted that released ions from HA affect electrostatics in non-negligible ways; therefore, the effective IS should be considered in DLVO calculations, particularly in low IS solutions.

Surface Potential. Surface potential measurements for all tested treatments, shown in Table 1, reveal that silver and mica surfaces are very highly charged ($|\psi_0| > 40$ mV) and require estimation of electrostatic interactions by NLPB, rather than well-known analytical approximations to DLVO theory (e.g., Hogg et al., 63 Wiese and Healy, 64 Bell et al. 65) that assume low potential ($|\psi_0|$ < 25 mV). Estimated ψ_0 values in the control solution, in the absence of HA, are in agreement with values reported in the literature. $\psi_0^{\rm M} = -110$ mV for mica is within the range reported by Israelachvili and Adams⁵⁸ of [-50, -130] mV, while $\psi_0^S = -50$ mV for silver is consistent with reported ζ -potential measurements of silver colloids and nanoparticles, 66,67 including our own collected values (see ζ_S in Table 1). Excellent agreement between SFA-determined ψ_0 and ζ -potential measurements demonstrates the statistical equivalence between the two methods. For the -HA solution, adsorption of negatively charged HA moieties onto silver and

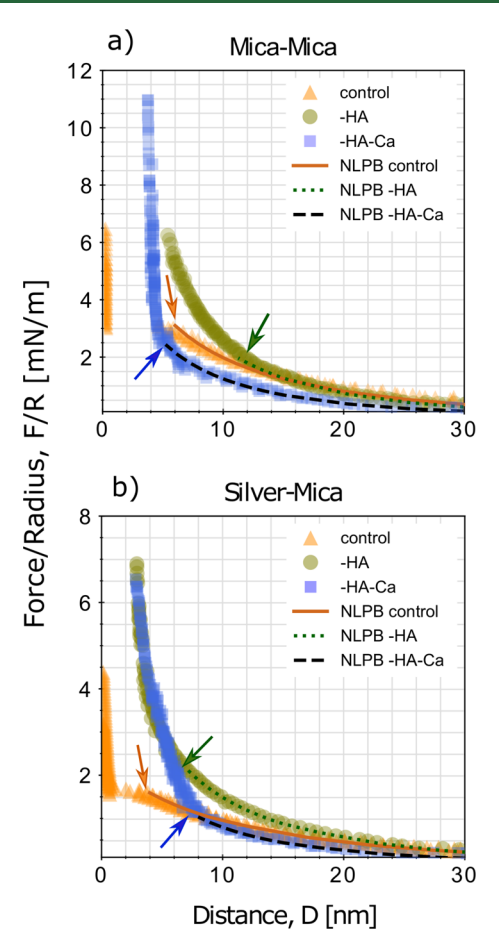


Figure 2. Force—distance profiles between opposing (a) mica—mica and (b) silver—mica surfaces. Markers correspond to the different solution conditions: control (orange triangles), -HA (green circles), and -HA-Ca (blue squares). Lines show the fit of the nonlinear Poisson—Boltzmann model at constant charge boundary conditions. Arrows indicate the onset of nonelectrostatic force at short separation distances.

mica surfaces resulted in more negative ψ_0 relative to that of experiments in the control solution. Adsorption of polydisperse macromolecules onto like-charged surfaces in the presence of monovalent ions has been reported before. We propose that the major mechanisms of adsorption in the -HA solution are charge screening by NaNO3 and attractive interactions between cations adsorbed on the negatively charged surfaces and the aromatic moieties in HA. The cation $-\pi$ interaction is well-recognized as an intermolecular, noncovalent attraction (including a substantial electrostatic component) between cations and aromatic π -systems, and it is comparable in strength to hydrogen bonding. For the -HA-Ca solution, ψ_0 on both surfaces was more neutral compared to that of the -HA solution. In this case, Ca²⁺ neutralized some functional groups by forming coordination complexes with ligands (e.g., HA, silver, and mica surfaces). 40 In both HA-containing solutions, the relative change in ψ_0 was larger on mica, which is more negatively charged than that on silver.

Magnitude and Origin of Nonelectrostatic Repulsive Forces. Quantitative evidence of nonelectrostatic repulsive forces are presented in this section. To verify that SFA measurements can be used to discern individual surface force contributions, we first presented evidence that total force, $F_{\rm T}$, in the control solution was captured by the summation of $F_{\rm VDW}$

and $F_{\rm EDL}$ alone (see $F_{\rm T}$ in inset of Figure 1). The total force in HA-containing solutions, however, shows that an additional repulsive force (generally considered of steric origin in the literature 40,60,72) significantly contributes toward $F_{\rm T}$. To determine the steric contribution from the adsorbed HA layers, the $F_{\rm VDW}$ and the fitted $F_{\rm EDL}$ were subtracted from $F_{\rm T}$. It is noteworthy that the presence of HA adsorbed layers prevented the surfaces from coming into contact as defined from the control solution (D=0). Moreover, the minimum separation distance for -HA and -HA-Ca solutions was the sum of the compressed layers on each surface, that is, $2L_{\rm M}{}'$ for the symmetric system and $L_{\rm M}{}' + L_{\rm S}{}'$ for the asymmetric system. At such separations, VDW interactions between the surfaces were essentially negligible. Figure 3 shows the magnitude of the

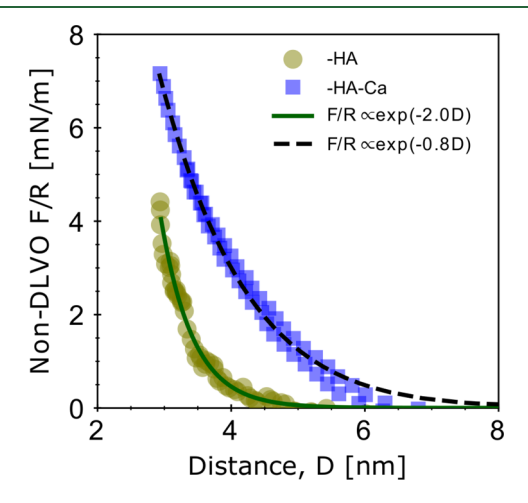


Figure 3. Non-DLVO force—distance profiles between opposing silver—mica surfaces in -HA (green circles) and -HA-Ca (blue squares) solutions. Solid and dashed lines show the exponential decay of the repulsive forces with distance.

remaining nonelectrostatic repulsive force in -HA and -HA-Ca solution conditions for the asymmetric mica—silver system. It is evident that this non-DLVO force decays exponentially with distance, with average rates of ~2.0 and 0.8 nm⁻¹ for -HA and -HA-Ca solutions, respectively. The faster decay rate for the -HA solution, compared to the -HA-Ca case, is consistent with the thinner but denser total adsorbed layer $(L_{\rm M} + L_{\rm S})$ in the former solution.⁷³

Certainty in the origin for each contributing surface force is necessary to make predictions of colloidal interactions in HArich systems that cannot be measured directly by, for example, SFA. Modeling approaches for calculating the structural forces brought about from HA sorption have been heavily based on soft particle theory (SPT). 72,74,75 However, SPT requires that three key conditions are met: the adsorbed macromolecules must be composed of many repeating subunits (> $O(10^2)$), polydispersity of the polymer must be low, and $L \gg \kappa^{-1}$. According to our measurements, none of these conditions are satisfied for HA adsorption layers on mica or silver. First, the molecular structure of HA is highly variable, making it unlikely that the adsorbed macromolecule assembles into long chains of at least hundreds of identically repeating units. Second, the polydispersity of HA is relatively high (1.76-2.5). 76,77 Highly polydispersed materials display a complex interplay between adsorption and configurational entropy. While larger molecules diffuse and equilibrate more slowly onto the surfaces, their

adsorption results in a more pronounced decrease in the interfacial energy and is thus favored at longer times. ^{78,79} Third, in all cases tested in this study, $L < \kappa^{-1}$ by at least a factor of 2, indicating that elastic—steric repulsion is negligible compared to osmotic—steric repulsion for HA. All together, these considerations suggest that Ohshima's soft particle theory is not appropriate for describing repulsive forces imparted by adsorbed HA. In sections following, we present quantitative evidence for the osmotic origin of extra repulsive forces in HA-rich systems.

Adsorbed Layer Properties. Experimental properties regarding adsorbed layer characteristics for each surface and solution tested are summarized in Table 1. In the control solution conditions, surfaces were bare, and all adsorbed layer properties are reported as zero.

Layer Thickness and Compressibility. Uncompressed adsorbed HA layer thickness, L, was determined by the distance where the force profile measurements deviated from the NLPB fit, as indicated by the arrows in Figure 2. The compressibility of the HA layers, λ , was estimated as $\lambda = (L L')/L \times 100$, where L' is the compressed layer thickness at a separation distance recorded for an applied force of 6 mN/m. At this range, an increase in applied force did not change the separation distance by more than 1 nm. The symmetric configuration was used to estimate HA layer thickness on one mica surface as L/2 in each solution. The asymmetric configuration then provided the layer thickness on the silver surface by subtracting the known thickness of the layer on mica from the measured L of the system. The same logic was used for the estimation of λ . Here, we interpret λ as a proxi of the density of the adsobed layer.

All measured uncompressed adsorption layers between approaching surfaces were thinner than the solution κ^{-1} . This facilitated fitting the system's electrostatics, which are dominant at D > 10 as L < 7 nm. By subtracting electrostatics and van der Waals from the total force profile, we distinguish the steric contribution from the adsorbed HA layers. For -HA solution conditions, the adsorbed layer on mica, $L_{\rm M}$, was an order of magnitude thicker than that on silver, L_S. In this solution, the compressibility of the adsorbed layers on silver and mica λ_S and λ_M , respectively, was close to 50%, suggesting an intermediate layer density that is independent of the substrate. For -HA-Ca solution conditions, $L_{\rm M}$ and $\lambda_{\rm M}$ were reduced, implying an increase in the HA layer density on mica, while L_S and λ_S increased, indicating that the layer on silver in the presence of calcium was thicker and more diffuse that the one on mica. At this solution, $L_{\rm M}$ and $L_{\rm S}$ were in the same order of magnitude.

Mass Adsorbed. Mass of HA adsorbed per unit surface area was obtained through the expression $\Gamma = \rho_{\rm HA} \phi L'$. $\rho_{\rm HA}$ is the HA density taken as 1.45 g/mL. 80 $\phi = 0.55$ is the volumetric fraction of HA to the solvent, from direct measurements of similarly polydispersed polymers in a good solvent at $F/R \sim 6$ mN/m. 81 Substantial differences in mass of adsorbed polymer per unit area, Γ , were observed across solution conditions. For the -HA solution, $\Gamma_{\rm M}$ was an order of magnitude greater than $\Gamma_{\rm S}$. Our estimate for $\Gamma_{\rm M}$ is in agreement with the report by Taunton et al. 82 for high molecular weight polymer adsorption onto mica in good solvent conditions. Our estimate for $\Gamma_{\rm S}$, however, was considerably lower than values reported elsewhere. 40 For the -HA-Ca solution, $\Gamma_{\rm S}$ significantly increased, suggesting that Ca^{2+} counterions promote adsorption of negatively charged HA onto like-charged silver. 83 We

point out that the value for Γ_M in -HA-Ca reported in Table 1 is different from what was determined based on this parameter's definition ($\Gamma_M = 1.54 \text{ mg/m}^2$). This original calculation would imply that desorption of HA happened in the presence of Ca^{2+} . We know this result to be incorrect. Rather, Ca^{2+} is expected to enhance HA adsorption and, most importantly, to increase the density of the existing adsorbed layer. Investigating the nature of this discrepancy is beyond the scope of this work, so we instead report the estimated value for Γ_M from -HA solutions again.

Deposition of Silver Nanoparticles in HA-Rich Porous Media. Nanoparticle deposition on micalike porous media at the solution conditions relevant to this study was investigated by estimations of the system's attachment efficiency, α , from colloid filtration theory (CFT). α is a kinetic transport parameter widely used to quantify the probability of a particle attaching to a soil grain after collision. To determine the best model for estimating α in each solution composition, it was first necessary to properly account for the different force contributors to the net interaction that describes the system. Here, we demonstrate that the interplay of the osmotic, electric double layer, and van der Waals forces is sufficient to capture the measured interactions.

Interaction Energy Translation. In environmental engineering applications, it is standard to employ energy of interaction profiles to justify deposition trends of colloids/nanoparticles transported in porous media. We used Derjaguin's approximation⁸⁴ to translate the force profiles between cross-cylinders of silver—mica surfaces from SFA measurements, F/R, into energy of interaction, W, between hypothetical cases of silver nanoparticles and mica collectors, viz.:

$$W(D) = -\frac{R_{\rm S}R_{\rm M}}{R_{\rm S} + R_{\rm M}} \int_{\infty}^{D} \frac{F}{R} \,\mathrm{d}D' \tag{4}$$

Here, $R_{\rm S}$ and $R_{\rm M}$ correspond to the radii of the (silver) nanoparticle and the (mica) collector, respectively. The translated profiles are considered empirical data for various scenarios of nanoparticle sizes. Furthermore, these data are used to gauge the relative effect of adsorbed HA on the energy of interaction between collectors and nanoparticles of different sizes.

To compleiment the empirical data, theoretical estimations of the total energy of interaction, $W_{\rm T}$, are provided with an extension to classic DLVO theory to account for osmotic repulsion⁸⁵ as per the following:

$$W_{\rm T} = W_{\rm EDL} + W_{\rm VDW} + W_{\rm OSM} \tag{5}$$

$$W_{\text{VDW}} = -\left(\frac{R_{\text{S}}R_{\text{M}}}{R_{\text{S}} + R_{\text{M}}}\right)\frac{A}{6D} \tag{6}$$

$$W_{\rm EDL} = \left(\frac{R_{\rm S}R_{\rm M}}{R_{\rm S} + R_{\rm M}}\right) \frac{2\pi}{\kappa} \text{NLPB}$$
 (7)

$$W_{\text{OSM}} = \begin{cases} 0 & D \ge 2\overline{L} \\ \left(\frac{R_{\text{S}}R_{\text{M}}}{R_{\text{S}} + R_{\text{M}}}\right) \frac{2\pi}{\nu_{1}} \Phi_{\text{S}} \Phi_{\text{M}} \left(\frac{1}{2} - \chi\right) & \overline{L} \le D < 2\overline{L} \end{cases}$$

$$\left(\overline{L} - \frac{D}{2}\right)^{2} \\ \left(\frac{R_{\text{S}}R_{\text{M}}}{R_{\text{S}} + R_{\text{M}}}\right) \frac{2\pi}{\nu_{1}} \Phi_{\text{S}} \Phi_{\text{M}} \left(\frac{1}{2} - \chi\right) \overline{L}^{2} \qquad D < \overline{L}$$

$$\left(\frac{D}{2\overline{L}} - \frac{1}{4} - \ln\left(\frac{D}{\overline{L}}\right)\right) \tag{8}$$

We consider that $R_{\rm S}=10$, 20, and 50 nm for different particle size scenarios. $W_{\rm EDL}$ was determined by numerically solving the Poisson–Boltzmann equation, because the surface charges exceeded the validity of well-knonwn analytical approximations for electric double layer energies. It should be noted that the set of expressions for $W_{\rm OSM}$ is adapted from an approximation for a symmetric system (Peter Kralchevsky, personal communication, 18 March 2020). Here, ν_1 is the volume of a solvent (water) molecule. χ is the Flory–Huggins solvency parameter. $\overline{L}=(L_{\rm M}+L_{\rm S})/2$ is the average adsorbed layer thickness. $\Phi_{\rm S}$ and $\Phi_{\rm M}$ are the volume fractions of the adsorbed HA layer onto silver and mica spheres, respectively, and are calculated as

$$\Phi = 3 \frac{\Gamma R^2}{\rho_{\text{HA}} [(L + R^3) - R^3]}$$
 (9)

Figure 4 shows very good agreement between model predictions for $W_{\rm T}$ (shaded region marking the boundary condition limits for constant charge and constant potential) and the empirical data (markers) under all particle sizes and all solution conditions. In estimating W_{OSM} , χ was treated as a free model parameter, and $\rho_{\rm HA}$ was fixed at 1.45 g/cm³ (a parameter the model was not sensitive to). It is worth noting that the peaks at $D \sim 4$ nm in model predictions for -HA solutions are due to the large difference between $L_{\rm M}$ and $L_{\rm S}$. This discrepancy creates a discontinuity in the individual expressions for $W_{\rm OSM}$, which is indistinguishable for the -HA-Ca solutions where $L_{\rm M}$ and $L_{\rm S}$ are within the same order of magnitude. The higher limit on the y-axis was fixed at 100 kT, because higher energy barriers are considered insurmountable with the particle's kinetic energy. The complete energy profile is shown in Figure S2. From this, it is evident that classic DLVO is insufficient to describe the system and that an osmotic contribution captures the physics of the additional repulsion imparted by HA adsorption well. Two notable trends are evident in Figure 4. First, the net energy of interaction scales with particle size, implying that inaccuracies in the modeled interaction energy are magnified with increasing particle size. Second, the energy barrier increases manyfold with solution composition complexity. That is, $W_{\rm T}^{\rm max}$ for control < -HA < -HA-Ca, making it imperative to ascertain the origin of non-DLVO forces in complex solutions. Estimations of the elastic-steric component of steric-type forces⁷² did not significantly contribute to the interaction profile and were confirmed negligible. As an additional reference, Figure S3 shows an equivalent comparison for predictions that considers only van der Waals and electrostatic energies, illustrating the need to include an additional osmotic force contribution.

Attachment Efficiency. CFT is commonly employed to describe transport kinetics of particle deposition in porous media in dimensionless terms from breakthrough data. Various

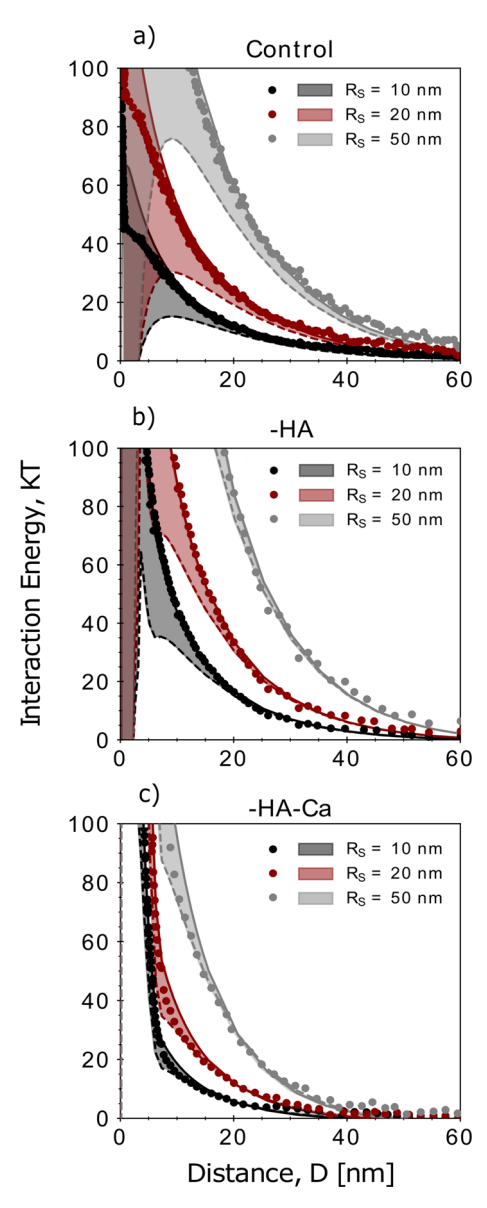


Figure 4. Total energy profiles $(W_{\rm T}=W_{\rm EDL}+W_{\rm VDW}+W_{\rm OSM})$ for interactions between silver particles and mica collectors in (a) control, (b) -HA, and (c) -HA-Ca solutions. Shaded regions show the model predictions with upper and lower limits for electrostatics corresponding to constant charge (solid line) and constant potential (dashed line), respectively. Empirical data (translated from SFA force measurements) is shown as symbols.

semiempirical correlations have been proposed to estimate the attachment efficiency, α , of colloidal suspensions colliding with simplified porous media. $^{28-31}$ However, there is no widely accepted unified mechanistic model for predicting α under unfavorable deposition conditions (i.e., with energy barriers high enough to prevent particle attachment). In the following, we employ the proposed correlation equation for bare electrostatically stabilized particles from Bai and Tien ²⁹ to predict the attachment efficiency of nanoparticle suspensions in the control solution ($\alpha_{\rm bare}$). Similarly, we use the correlation equation for surface-coated electrosterically stabilized particles from Phenrat et al. ³⁰ to predict the attachment efficiency of nanoparticles in the -HA and -HA-Ca solutions ($\alpha_{\rm coat}$). Details about α calculations are provided in the Supporting Information.

Predictions for α corresponding to the interaction energy profiles in the previous section are shown in Figure 5. The

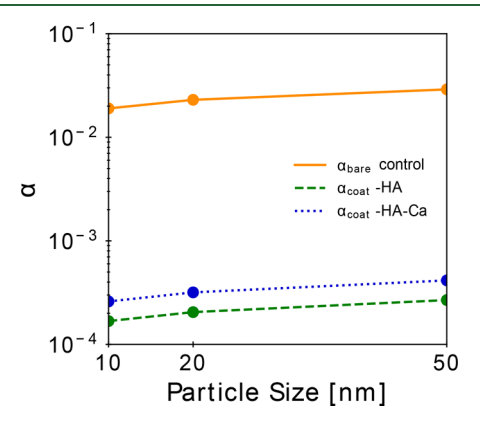


Figure 5. Estimated attachment efficiency, α , for suspensions of variably sized particles colliding with simplified porous media at different solution conditions. The solid line considers the dimensionless semiempirical correlation for electrostatically stabilized suspensions (without surface coatings) from Bai and Tien. Dashed lines consider the correlation for electrosterically stabilized suspensions (afforded by adsorbed macromolecules) from Phenrat et al. Dashed lines

results are in qualitative agreement with experimental α values resulting from transport tests of silver nanoparticle suspensions in monovalent salt, in the presence of HA, and in solutions containing HA and divalent cations. $^{86-88}$ It is evident that α increases monotonically with particle size in both bare and surface-coated model correlations. For particles of equivalent size, $\alpha_{\rm bare}$ was much larger than $\alpha_{\rm coat}$ at ${\cal O}(10^{-2})$ and ${\cal O}(10^{-4})$, respectively. This is consistent with the lowest energy barrier found $(O(10^1 - 10^2) \text{ kT}$, see Figure S1) for the control solution, where only electrostatics create unfavorable conditions. Similar values for α_{coat} were found for particles of equivalent size in solution conditions that promote surface coatings. Efficiencies in -HA were slightly smaller than those in -HA-Ca solutions, which cannot be explained by trends in the energy barrier magnitude at $O(10^2 - 10^3)$ kT (see Figure S1). Simply, the energy barrier afforded by adsorbed HA macromolecules is equally insurmountable in -HA as in -HA-Ca solutions. We propose that differences in $\alpha_{\rm coat}$ are better attributed to the secondary energy well, which is entirely absent for -HA solutions and present for -HA-Ca with a deep enough minimum (\leq deeper than 5 kT) for particles $R_S \geq 50$ nm (see Figure S4). This implies that, within the geometry of porous media, retention in secondary energy minima in the presence of an insurmountable energy barrier would likley cause particles to accumulate at grain-to-grain contacts. Despite the reasonable agreement found between our authenticated energy of interaction profiles and the predictions for α , additional work is needed to (i) confirm that elastic forces are negligible for a broader range of DOM conditions than those tested here and, if confirmed, (ii) revise the correlation for α_{coat} to give greater importance to the osmotic component over the elastic one for steric repulsion.

Technical and Environmental Implications for Colloid Transport. This work investigated the surface interactions between charged silver and mica substrates in various solution compositions relevant to agricultural soils. We confirmed that, in the absence of HA, the forces at play are electrostatic repulsion and van der Waals attraction. Once the surfaces are

exposed to DOM, macromolecules like HA readily adsorb onto both materials. However, important differences on the adsorbed layers were found. On mica, the HA layer was thicker, more charged, and more dense than the one observed on silver. Additionally, changes in the effective solution IS from ionization of the HA moieties were detected, which affect the overall system's electrostatics. When the solution complexity was increased by including calcium ions, the differences in adsorbed layer thickness and charge between mica and silver were reduced. The data indicate that calcium ions promote a greater adsorbed mass and increase the HA layer thickness for silver but increase the HA layer density for mica.

Our measurements suggest that HA has the potential to influence the deposition of n-Ag particles onto soil grains in three key ways: (i) by changing the electrical double layer forces, (ii) by creating a physical barrier between particles and collectors, and (iii) by generating additional interactions due to compression of the HA adsorbed layers, as reflected in the measured force profiles and estimated energy profiles. Based on our calculations, the probability of particle deposition (α) is expected to be the lowest in HA-rich solutions, relative to the other solutions tested. In order to extend the use of the CFT to model ENPs filtration in HA-rich solutions, the osmotic repulsion arising from the overlap of adsorbed HA layers must be considered in addition to electrostatic and van der Waals interactions (classic DLVO theory). Because HA and other DOM macromolecules are ubiquitous in soil, especially in agricultural soils, these results imply that HA-coated ENPs may travel much farther than their bare counterparts, potentially reaching sensitive water resources. While this conclusion is based on ideal and smooth surfaces, the authors recognize that the combined effect of adsorbed natural macromolecules, 86,88 heterogeneity of the soil surface that creates favorable microsites for deposition, $^{90-93}$ and heteroaggregation 94,95 may reduce the expected travel distances of ENPs. Nonetheless, our study demonstrates that osmotic repulsion from adsorbed DOM onto suspensions and collectors is the main factor controlling interactions between ENPs and soil surfaces and, consequently, their probability for deposition. Precise characterization of the relevant surface coating properties on natural and engineered materials is a first step toward improving the accuracy of predictive models for colloid transport in the subsurface.

ASSOCIATED CONTENT

Supporting Information

The Supporting Information is available free of charge at https://pubs.acs.org/doi/10.1021/acs.est.0c05334.

Debye length from force measurements; full energy profiles based on xDLVO; energy predictions based on DLVO; attachment efficiency, α , calculations; and secondary energy wells from experimental data (PDF)

AUTHOR INFORMATION

Corresponding Author

Verónica L. Morales — Department of Civil and Environmental Engineering, University of California, Davis, California 95616, United States; ⊙ orcid.org/0000-0002-9595-6026; Phone: +1 (530) 752-4008; Email: vermorales@ucdavis.edu

Authors

Janis E. Patiño – Department of Civil and Environmental Engineering, University of California, Davis, California 95616, United States

Tonya L. Kuhl — Department of Chemical Engineering, University of California, Davis, California 95616, United States; orcid.org/0000-0002-6069-0205

Complete contact information is available at: https://pubs.acs.org/10.1021/acs.est.0c05334

Notes

The authors declare no competing financial interest.

ACKNOWLEDGMENTS

This work was funded in part by the U.S. NSF (EAR-1847689), the Hellman Fellowship, and the P.E.O. International Peace Scholarship. Acknowledgment is made to the Donors of the American Chemical Society Petroleum Research Fund (59864-DNI9 and 59-483-ND5) for partial support of this research.

REFERENCES

- (1) Keller, A. A.; Vosti, W.; Wang, H.; Lazareva, A. Release of engineered nanomaterials from personal care products throughout their life cycle. *J. Nanopart. Res.* **2014**, *16*, 2489.
- (2) Gottschalk, F.; Sun, T.; Nowack, B. Environ. concentrations of engineered nanomaterials: review of modeling and analytical studies. *Environ. Pollut.* **2013**, *181*, 287–300.
- (3) Benn, T. M.; Westerhoff, P. Nanoparticle silver released into water from commercially available sock fabrics. *Environ. Sci. Technol.* **2008**, *42*, 4133–4139.
- (4) Goswami, L.; Kim, K.-H.; Deep, A.; Das, P.; Bhattacharya, S. S.; Kumar, S.; Adelodun, A. A. Engineered nano particles: nature, behavior, and effect on the environment. *J. Environ. Manage.* **2017**, 196, 297–315.
- (5) Balantrapu, K.; Goia, D. V. Silver nanoparticles for printable electronics and biological applications. *J. Mater. Res.* **2009**, *24*, 2828–2836.
- (6) Sondi, I.; Salopek-Sondi, B. Silver nanoparticles as antimicrobial agent: a case study on E. coli as a model for Gram-negative bacteria. *J. Colloid Interface Sci.* **2004**, *275*, 177–182.
- (7) Maillard, J.-Y.; Hartemann, P. Silver as an antimicrobial: facts and gaps in knowledge. *Crit. Rev. Microbiol.* **2013**, *39*, 373–383.
- (8) Zhang, C.; Hu, Z.; Deng, B. Silver nanoparticles in aquatic environments: Physiochemical behavior and antimicrobial mechanisms. *Water Res.* **2016**, *88*, 403–427.
- (9) Kaegi, R.; Voegelin, A.; Sinnet, B.; Zuleeg, S.; Hagendorfer, H.; Burkhardt, M.; Siegrist, H. Behavior of metallic silver nanoparticles in a pilot wastewater treatment plant. *Environ. Sci. Technol.* **2011**, *45*, 3902–3908.
- (10) Benn, T.; Cavanagh, B.; Hristovski, K.; Posner, J. D.; Westerhoff, P. The release of nanosilver from consumer products used in the home. *J. Environ. Qual.* **2010**, *39*, 1875–1882.
- (11) McGrath, S.; Chang, A.; Page, A.; Witter, E. Land application of sewage sludge: scientific perspectives of heavy metal loading limits in Europe and the United States. *Environ. Rev.* **1994**, *2*, 108–118.
- (12) Blaser, S. A.; Scheringer, M.; MacLeod, M.; Hungerbühler, K. Estimation of cumulative aquatic exposure and risk due to silver: contribution of nano-functionalized plastics and textiles. *Sci. Total Environ.* **2008**, 390, 396–409.
- (13) Gajjar, P.; Pettee, B.; Britt, D. W.; Huang, W.; Johnson, W. P.; Anderson, A. J. Antimicrobial activities of commercial nanoparticles against an environmental soil microbe, Pseudomonas putida KT2440. *J. Biol. Eng.* **2009**, *3*, 1–13.
- (14) Dimkpa, C.; Calder, A.; Gajjar, P.; Merugu, S.; Huang, W.; Britt, D.; McLean, J.; Johnson, W.; Anderson, A. Interaction of silver

- nanoparticles with an environmentally beneficial bacterium, Pseudomonas chlororaphis. *J. Hazard. Mater.* **2011**, *188*, 428–435.
- (15) Mijnendonckx, K.; Leys, N.; Mahillon, J.; Silver, S.; Van Houdt, R. Antimicrobial silver: uses, toxicity and potential for resistance. *BioMetals* **2013**, 26, 609–621.
- (16) Beer, C.; Foldbjerg, R.; Hayashi, Y.; Sutherland, D. S.; Autrup, H. Toxicity of silver nanoparticles—nanoparticle or silver ion? *Toxicol. Lett.* **2012**, *208*, 286–292.
- (17) Calder, A. J.; Dimkpa, C. O.; McLean, J. E.; Britt, D. W.; Johnson, W.; Anderson, A. J. Soil components mitigate the antimicrobial effects of silver nanoparticles towards a beneficial soil bacterium, Pseudomonas chlororaphis O6. *Sci. Total Environ.* **2012**, 429, 215–222.
- (18) Tufenkji, N.; Elimelech, M. Correlation equation for predicting single-collector efficiency in physicochemical filtration in saturated porous media. *Environ. Sci. Technol.* **2004**, *38*, 529–536.
- (19) Yao, K.-M.; Habibian, M. T.; O'Melia, C. R. Water and waste water filtration. Concepts and applications. *Environ. Sci. Technol.* **1971**, *5*, 1105–1112.
- (20) Derjaguin, B.; Landau, L. Theory of the Stability of Strongly Charged Lyophobic Sols and of the Adhesion of Strongly Charged Particles in Solutions of Electrolytes. *Acta Physicochim. URSS* **1941**, *14*. 633–662.
- (21) Verwey, E. J. W.; Overbeek, J. T. G.; Van Nes, K. Theory of the Stability of Lyophobic Colloids: The Interaction of Sol Particles Having an Electric Double Layer; Elsevier Publishing Company, 1948.
- (22) Ohshima, H. Theory of electrostatics and electrokinetics of soft particles. *Sci. Technol. Adv. Mater.* **2009**, *10*, No. 063001.
- (23) Grasso, D.; Subramaniam, K.; Butkus, M.; Strevett, K.; Bergendahl, J. A review of non-DLVO interactions in environmental colloidal systems. *Rev. Environ. Sci. Bio/Technol.* **2002**, *1*, 17–38.
- (24) Dwivedi, A. D.; Dubey, S. P.; Sillanpää, M.; Kwon, Y.-N.; Lee, C.; Varma, R. S. Fate of engineered nanoparticles: implications in the environment. *Coord. Chem. Rev.* **2015**, 287, 64–78.
- (25) Harvey, R. W.; Garabedian, S. P. Use of colloid filtration theory in modeling movement of bacteria through a contaminated sandy aquifer. *Environ. Sci. Technol.* **1991**, *25*, 178–185.
- (26) Ryan, J. N.; Elimelech, M. Colloid mobilization and transport in groundwater. *Colloids Surf.*, A **1996**, 107, 1–56.
- (27) Ma, H.; Hradisky, M.; Johnson, W. P. Extending applicability of correlation equations to predict colloidal retention in porous media at low fluid velocity. *Environ. Sci. Technol.* **2013**, *47*, 2272–2278.
- (28) Elimelech, M. Predicting collision efficiencies of colloidal particles in porous media. *Water Res.* **1992**, *26*, 1–8.
- (29) Bai, R.; Tien, C. A new correlation for the initial filter coefficient under unfavorable surface interactions. *J. Colloid Interface Sci.* 1996, 179, 631–634.
- (30) Phenrat, T.; Song, J. E.; Cisneros, C. M.; Schoenfelder, D. P.; Tilton, R. D.; Lowry, G. V. Estimating attachment of nano-and submicrometer-particles coated with organic macromolecules in porous media: development of an empirical model. *Environ. Sci. Technol.* **2010**, *44*, 4531–4538.
- (31) Morales, V. L.; Sang, W.; Fuka, D. R.; Lion, L. W.; Gao, B.; Steenhuis, T. S. Correlation equation for predicting attachment efficiency (α) of organic matter-colloid complexes in unsaturated porous media. *Environ. Sci. Technol.* **2011**, *45*, 10096–10101.
- (32) Shen, C.; Li, B.; Huang, Y.; Jin, Y. Kinetics of coupled primaryand secondary-minimum deposition of colloids under unfavorable chemical conditions. *Environ. Sci. Technol.* **2007**, *41*, 6976–6982.
- (33) Aiken, G. R.; Hsu-Kim, H.; Ryan, J. N. Influence of dissolved organic matter on the environmental fate of metals, nanoparticles, and colloids. *Environ. Sci. Technol.* **2011**, *45*, 3196–3201.
- (34) Grillo, R.; Rosa, A. H.; Fraceto, L. F. Engineered nanoparticles and organic matter: a review of the state-of-the-art. *Chemosphere* **2015**, *119*, 608–619.
- (35) Louie, S. M.; Tilton, R. D.; Lowry, G. V. Effects of molecular weight distribution and chemical properties of natural organic matter on gold nanoparticle aggregation. *Environ. Sci. Technol.* **2013**, 47, 4245–4254.

- (36) Stankus, D. P.; Lohse, S. E.; Hutchison, J. E.; Nason, J. A. Interactions between natural organic matter and gold nanoparticles stabilized with different organic capping agents. *Environ. Sci. Technol.* **2011**, *45*, 3238–3244.
- (37) Zhang, Y.; Chen, Y.; Westerhoff, P.; Crittenden, J. Impact of natural organic matter and divalent cations on the stability of aqueous nanoparticles. *Water Res.* **2009**, *43*, 4249–4257.
- (38) Chen, K. L.; Elimelech, M. Influence of humic acid on the aggregation kinetics of fullerene (C60) nanoparticles in monovalent and divalent electrolyte solutions. *J. Colloid Interface Sci.* **2007**, 309, 126–134.
- (39) Saleh, N. B.; Pfefferle, L. D.; Elimelech, M. Aggregation kinetics of multiwalled carbon nanotubes in aquatic systems: measurements and environmental implications. *Environ. Sci. Technol.* **2008**, *42*, 7963–7969.
- (40) Morales, V. L.; Zhang, W.; Gao, B.; Lion, L. W.; Bisogni, J. J., Jr; McDonough, B. A.; Steenhuis, T. S. Impact of dissolved organic matter on colloid transport in the vadose zone: deterministic approximation of transport deposition coefficients from polymeric coating characteristics. *Water Res.* **2011**, *45*, 1691–1701.
- (41) Thio, B. J. R.; Montes, M. O.; Mahmoud, M. A.; Lee, D.-W.; Zhou, D.; Keller, A. A. Mobility of capped silver nanoparticles under environmentally relevant conditions. *Environ. Sci. Technol.* **2012**, *46*, 6985–6991.
- (42) Chen, K. L.; Elimelech, M. Interaction of Fullerene (C-60) Nanoparticles with Humic Acid and Alginate Coated Silica Surfaces: Measurements, Mechanisms, and Environmental Implications. *Environ. Sci. Technol.* **2008**, *42*, 7607–7614.
- (43) Adrian, Y. F.; Schneidewind, U.; Bradford, S. A.; Simunek, J.; Fernandez-Steeger, T. M.; Azzam, R. Transport and retention of surfactant-and polymer-stabilized engineered silver nanoparticles in silicate-dominated aquifer material. *Environ. Pollut.* **2018**, 236, 195–207.
- (44) Hoppe, M.; Mikutta, R.; Utermann, J.; Duijnisveld, W.; Guggenberger, G. Retention of sterically and electrosterically stabilized silver nanoparticles in soils. *Environ. Sci. Technol.* **2014**, 48, 12628–12635.
- (45) Kanel, S. R.; Flory, J.; Meyerhoefer, A.; Fraley, J. L.; Sizemore, I. E.; Goltz, M. N. Influence of natural organic matter on fate and transport of silver nanoparticles in saturated porous media: laboratory experiments and modeling. *J. Nanopart. Res.* **2015**, *17*, 154.
- (46) Li, Z.; Greden, K.; Alvarez, P. J.; Gregory, K. B.; Lowry, G. V. Adsorbed polymer and NOM limits adhesion and toxicity of nano scale zerovalent iron to E. coli. *Environ. Sci. Technol.* **2010**, *44*, 3462–3467
- (47) Furman, O.; Usenko, S.; Lau, B. L. Relative importance of the humic and fulvic fractions of natural organic matter in the aggregation and deposition of silver nanoparticles. *Environ. Sci. Technol.* **2013**, 47, 1349–1356.
- (48) Sander, S.; Mosley, L. M.; Hunter, K. A. Investigation of interparticle forces in natural waters: Effects of adsorbed humic acids on iron oxide and alumina surface properties. *Environ. Sci. Technol.* **2004**, 38, 4791–4796.
- (49) Fairhurst, A. J.; Warwick, P. The influence of humic acid on europium—mineral interactions. *Colloids Surf.*, A 1998, 145, 229–234.
- (50) Assemi, S.; Nalaskowski, J.; Johnson, W. P. Direct force measurements between carboxylate-modified latex microspheres and glass using atomic force microscopy. *Colloids Surf., A* **2006**, 286, 70–77
- (51) Kuhl, T.; Leckband, D. E.; Lasic, D.; Israelachvili, J. Modulation of interaction forces between bilayers exposing short-chained ethylene oxide headgroups. *Biophys. J.* **1994**, *66*, 1479–1488.
- (52) Boggs, S., Jr.; Livermore, D.; Seitz, M. G. Humic Substances in Natural Waters and Their Complexation with Trace Metals and Radionuclides: A Review. [129 references]; ANL-84-78 and ON: DE85015539; United States, 1985. DOI: 10.2172/5569909.
- (53) Israelachvili, J. N. Intermolecular and Surface Forces; Academic Press, 2015.

- (54) Israelachvili, J. Thin film studies using multiple-beam interferometry. J. Colloid Interface Sci. 1973, 44, 259–272.
- (55) Kurniawan, J.; Yin, N.-N.; Liu, G.-y.; Kuhl, T. L. Interaction forces between ternary lipid bilayers containing cholesterol. *Langmuir* **2014**, *30*, 4997–5004.
- (56) Ron, C. A.; VanNess, K.; Rasmuson, A.; Johnson, W. P. How nanoscale surface heterogeneity impacts transport of nano-to microparticles on surfaces under unfavorable attachment conditions. *Environ. Sci.: Nano* **2019**, *6*, 1921–1931.
- (57) Rojas, O. J. Adsorption of polyelectrolytes on mica. *Encyclopedia of Surface and Colloid Sci.* **2002**, *1*, 517–535.
- (58) Israelachvili, J. N.; Adams, G. E. Measurement of forces between two mica surfaces in aqueous electrolyte solutions in the range 0–100 nm. *J. Chem. Soc., Faraday Trans.* 1 1978, 74, 975–1001.
- (59) Grabbe, A. Double layer interactions between silylated silica surfaces. *Langmuir* **1993**, *9*, 797–801.
- (60) Elimelech, M.; Gregory, J.; Jia, X. Particle Deposition and Aggregation: Measurement, Modelling and Simulation; Butterworth-Heinemann, 2013.
- (61) Levins, J.; Vanderlick, T. Characterization of the interface between a rough metal and smooth mica in contact. *J. Colloid Interface Sci.* 1997, 185, 449–458.
- (62) Lifshitz, I.; Kosevich, A. Theory of magnetic susceptibility in metals at low temperatures. *Sov. Phys. JETP* **1956**, *2*, 636–645.
- (63) Hogg, R.; Healy, T. W.; Fuerstenau, D. W. Mutual coagulation of colloidal dispersions. *Trans. Faraday Soc.* **1966**, *62*, 1638–1651.
- (64) Wiese, G.; Healy, T. W. Effect of particle size on colloid stability. *Trans. Faraday Soc.* **1970**, *66*, 490–499.
- (65) Bell, G.; Levine, S.; McCartney, L. Approximate methods of determining the double-layer free energy of interaction between two charged colloidal spheres. *J. Colloid Interface Sci.* **1970**, 33, 335–359.
- (66) Klitzke, S.; Metreveli, G.; Peters, A.; Schaumann, G. E.; Lang, F. The fate of silver nanoparticles in soil solution Usorption of solutes and aggregation. *Sci. Total Environ.* **2015**, *535*, 54–60.
- (67) Haider, M. J.; Mehdi, M. S. Study of morphology and zeta potential analyzer for the silver nanoparticles. *Int. J. Sci. Eng. Res.* **2014**, *5*, 381–385.
- (68) Maroni, P.; Montes Ruiz-Cabello, F. J.; Cardoso, C.; Tiraferri, A. Adsorbed mass of polymers on self-assembled monolayers: Effect of surface chemistry and polymer charge. *Langmuir* **2015**, *31*, 6045–6054.
- (69) Moazzami-Gudarzi, M.; Maroni, P.; Borkovec, M.; Trefalt, G. Depletion and double layer forces acting between charged particles in solutions of like-charged polyelectrolytes and monovalent salts. *Soft Matter* **2017**, *13*, 3284–3295.
- (70) Kearney, P. C.; Mizoue, L. S.; Kumpf, R. A.; Forman, J. E.; McCurdy, A.; Dougherty, D. A. Molecular recognition in aqueous media. New binding studies provide further insights into the cation-pi. interaction and related phenomena. *J. Am. Chem. Soc.* **1993**, *115*, 9907–9919.
- (71) Dougherty, D. A. The cation- π interaction. Acc. Chem. Res. **2013**, 46, 885–893.
- (72) Phenrat, T.; Saleh, N.; Sirk, K.; Kim, H.-J.; Tilton, R. D.; Lowry, G. V. Stabilization of aqueous nanoscale zerovalent iron dispersions by anionic polyelectrolytes: adsorbed anionic polyelectrolyte layer properties and their effect on aggregation and sedimentation. *J. Nanopart. Res.* **2008**, *10*, 795–814.
- (73) Kuhl, T.; Leckband, D.; Lasic, D.; Israelachvili, J. Modulation and Modeling of Interaction Forces between Lipid Bilayers Exposing Terminally Grafted Polymer Chains; CRC Press: Boca Raton, FL, 1995.
- (74) Zhang, W.; Rattanaudompol, U.-s.; Li, H.; Bouchard, D. Effects of humic and fulvic acids on aggregation of aqu/nC60 nanoparticles. *Water Res.* **2013**, *47*, 1793–1802.
- (75) Louie, S. M.; Phenrat, T.; Small, M. J.; Tilton, R. D.; Lowry, G. V. Parameter identifiability in application of soft particle electrokinetic theory to determine polymer and polyelectrolyte coating thicknesses on colloids. *Langmuir* **2012**, *28*, 10334–10347.
- (76) Ren, S.; Tombacz, E.; Rice, J. A. Dynamic light scattering from power-law polydisperse fractals: Application of dynamic scaling to

- humic acid. Phys. Rev. E: Stat. Phys., Plasmas, Fluids, Relat. Interdiscip. Top. 1996, 53, 2980.
- (77) Chin, Y.-P.; Aiken, G.; O'Loughlin, E. Molecular weight, polydispersity, and spectroscopic properties of aquatic humic substances. *Environ. Sci. Technol.* **1994**, 28, 1853–1858.
- (78) Tiraferri, A.; Maroni, P. Rapid Desorption of Polyelectrolytes from Solid Surfaces Induced by Changes of Aqueous Chemistry. *Langmuir* **2018**, *34*, 12302–12309.
- (79) van Heiningen, J. A.; Hill, R. J. Poly (ethylene oxide) adsorption onto and desorption from silica microspheres: New insights from optical tweezers electrophoresis. *Macromolecules* **2011**, 44, 8245–8260.
- (80) Relan, P.; Girdhar, K.; Khanna, S. Molecular configuration of compost's humic acid by viscometric studies. *Plant Soil* **1984**, *81*, 203–208
- (81) Liao, W.-P.; Elliott, I. G.; Faller, R.; Kuhl, T. L. Normal and shear interactions between high grafting density polymer brushes grown by atom transfer radical polymerization. *Soft Matter* **2013**, *9*, 5753–5761.
- (82) Taunton, H. J.; Toprakcioglu, C.; Fetters, L. J.; Klein, J. Interactions between surfaces bearing end-adsorbed chains in a good solvent. *Macromolecules* **1990**, *23*, 571–580.
- (83) Tiraferri, A.; Maroni, P.; Borkovec, M. Adsorption of polyelectrolytes to like-charged substrates induced by multivalent counterions as exemplified by poly (styrene sulfonate) and silica. *Phys. Chem. Chem. Phys.* **2015**, *17*, 10348–10352.
- (84) Derjaguin, B. Friction and adhesion. IV. The theory of adhesion of small particles. *Colloid Polym. Sci.* **1934**, *69*, 155–164.
- (85) Vincent, B.; Edwards, J.; Emmett, S.; Jones, A. Depletion flocculation in dispersions of sterically-stabilised particles (S"soft spheres"). *Colloids Surf.* **1986**, *18*, 261–281.
- (86) Huynh, K. A.; Chen, K. L. Aggregation kinetics of citrate and polyvinylpyrrolidone coated silver nanoparticles in monovalent and divalent electrolyte solutions. *Environ. Sci. Technol.* **2011**, 45, 5564–5571.
- (87) Lin, S.; Cheng, Y.; Bobcombe, Y.; Jones, K. L.; Liu, J.; Wiesner, M. R. Deposition of silver nanoparticles in geochemically heterogeneous porous media: predicting affinity from surface composition analysis. *Environ. Sci. Technol.* **2011**, *45*, 5209–5215.
- (88) Yang, X.; Lin, S.; Wiesner, M. R. Influence of natural organic matter on transport and retention of polymer coated silver nanoparticles in porous media. *J. Hazard. Mater.* **2014**, 264, 161–168.
- (89) Johnson, W. P.; Tong, M.; Li, X. On colloid retention in saturated porous media in the presence of energy barriers: The failure of α , and opportunities to predict η . Water Resour. Res. 2007, 43, W12S13.
- (90) Johnson, P. R.; Sun, N.; Elimelech, M. Colloid transport in geochemically heterogeneous porous media: Modeling and measurements. *Environ. Sci. Technol.* **1996**, *30*, 3284–3293.
- (91) Elimelech, M.; Nagai, M.; Ko, C.-H.; Ryan, J. N. Relative insignificance of mineral grain zeta potential to colloid transport in geochemically heterogeneous porous media. *Environ. Sci. Technol.* **2000**, 34, 2143–2148.
- (92) Petosa, A. R.; Jaisi, D. P.; Quevedo, I. R.; Elimelech, M.; Tufenkji, N. Aggregation and deposition of engineered nanomaterials in aquatic environments: role of physicochemical interactions. *Environ. Sci. Technol.* **2010**, *44*, 6532–6549.
- (93) Pazmino, E.; Trauscht, J.; Dame, B.; Johnson, W. P. Power law size-distributed heterogeneity explains colloid retention on soda lime glass in the presence of energy barriers. *Langmuir* **2014**, *30*, 5412–5421.
- (94) Huynh, K. A.; McCaffery, J. M.; Chen, K. L. Heteroaggregation of multiwalled carbon nanotubes and hematite nanoparticles: rates and mechanisms. *Environ. Sci. Technol.* **2012**, *46*, 5912–5920.
- (95) Cornelis, G.; Pang, L.; Doolette, C.; Kirby, J. K.; McLaughlin, M. J. Transport of silver nanoparticles in saturated columns of natural soils. *Sci. Total Environ.* **2013**, *463*, 120–130.